

LASER SPECTROSCOPY OF  
DEUTERATED TRIATOMIC HYDROGEN MOLECULAR IONS

JOW-TSONG SHY, ROBERT DESERIO, JOHN W. FARLEY AND  
WILLIAM H. WING

PHYSICS DEPARTMENT, OPTICAL SCIENCES CENTER,  
AND ARIZONA RESEARCH LABORATORIES  
UNIVERSITY OF ARIZONA, TUCSON, ARIZONA 85721 U.S.A.

*in*

*Proceedings of the 1983 International School and Symposium on  
Precision Measurement and Gravity Experiment, Taipei, Republic of  
China, January 24 - February 2, 1983, ed. by W.-T. Ni (Published  
by National Tsing Hua University, Hsinchu, Taiwan, Republic of  
China, June, 1983)*

OUTLINE

Abstract .....	295
I. Introduction .....	295
A. History	
B. Importance	
II. Experiments of the Structure of $H_3^+$ .....	297
A. Beam-foil-induced dissociation	
B. Rydberg state emission spectra of neutral $H_3$ and $D_3$	
C. Infrared spectrum of $H_3^+$	
D. Infrared spectrum of $H_3^+$ , $D_2H^+$ and $D_3^+$ at dissociation limit	
III. Apparatus and Procedures .....	299
A. Ion source and population distributions	
B. Doppler tuning	
C. CO laser	
D. Choice of target gas	
E. Multiplicity advantage	
IV. Data Analysis and Experimental Results .....	307
A. $D_3^+$	
B. $HD_2^+$	
C. $H_2D^+$	
V. Conclusion .....	320
Acknowledgements .....	321
References .....	322

## LASER SPECTROSCOPY OF DEUTERATED TRIATOMIC HYDROGEN MOLECULAR IONS

Jow-Tsong Shy\*, Robert DeSerio, John W. Farley<sup>†</sup> and William H. WingDepartment of Physics, Optical Sciences Center and Arizona  
Research Laboratory, Tucson, AZ 85721, U.S.A.Abstract

Forty-five transitions of  $D_3^+$ , thirty-one transitions of  $HD_2^+$  and nine transitions of  $H_2D^+$  between 1650 and 2000  $\text{cm}^{-1}$  have been observed by the Doppler-tuned fast-ion-beam laser-spectroscopic method and measured to an error within 0.0045  $\text{cm}^{-1}$ . The history of the  $H_3^+$  problem, the importance of its stable isotopes to other field of sciences and the other main experiments are briefly reviewed and followed by a detailed discussion of our method and experimental results. Preliminary identification of the observed transitions are also included.

I. Introduction

## A. History

$H_3^+$  has been known to mass spectroscopists since J. J. Thomson<sup>1</sup> discovered it with his cathode ray tube apparatus in 1912. His experiments<sup>2</sup> seemed to indicate that  $H_3$  is a stable gas in which  $H_3^+$  can be formed by ionization. In 1916, Dempster<sup>3</sup> studied  $H_3^+$  yield as a function of  $H_2$  pressure in a mass spectrometer and showed that  $H_3^+$  is formed from a secondary reaction and is the dominant ion at high pressure. He found no evidence of a stable  $H_3$  molecule. Later, the dominant production reaction of  $H_3^+$



was studied experimentally by T.R. Hogness and E.G. Lunn<sup>4</sup> in 1925.

Despite its relative simplicity and early theoretical studies<sup>5,6</sup> there had been very little theoretical and experimental work done on its structure until 1957. This is apparently the cause of the remark attributed to H. Eyring<sup>7</sup> in 1957 that  $H_3^+$  was the "scandal of modern chemistry." Since Eyring's remark, a considerable amount of theoretical work has been done on the  $H_3^+$  electronic ground state.<sup>8</sup> Its structure was determined to be an equilateral triangle with bond length about 0.875 Å. There has been, however, very little experimental work on the structure of this fundamental ion. A careful spectroscopic examination of a hydrogen discharge plasma by Herzberg<sup>9</sup> in 1967 showed nothing in the visible or uv range that could be assigned to  $H_3^+$ .

Technological breakthroughs in the areas of electronics, computer science, and molecular beams and the evolution of laser sources in the last decade have spurred the spectroscopic studies (both theoretical and experimental) on molecular ions. The first careful *ab initio* calculations of the vibration-rotational spectra of  $\text{H}_3^+$  and its deuterated species were carried out by Carney and Porter in 1976<sup>10,11</sup>. The experimental confirmation of the equilateral triangle structure of  $\text{H}_3^+$  was done by three different groups<sup>12</sup> in 1978 with a novel beam-foil method. In 1979, Herzberg<sup>13</sup> observed the electronic emission spectra of excited neutral  $\text{H}_3$  and  $\text{D}_3$  molecules, consisting of an  $\text{H}_3^+$  or  $\text{D}_3^+$  core in its electronic ground state to which is loosely bound an electron in a Rydberg orbital. The spectra exhibited the perturbed vibration-rotational structure of the core ions.

The first direct spectroscopic observation of the  $\text{D}_3^+$  ion was made by our group in 1980<sup>14</sup> using the fast-beam laser spectroscopic method we had developed and applied previously to the spectroscopy of the  $\text{HD}^+$ <sup>15</sup> and  $^4\text{HeH}^+$ <sup>16</sup> ions. Eight vibration-rotational transitions were measured to an absolute frequency accuracy of 0.3 ppm. Four of these were assigned by Porter<sup>11</sup> to the  $\nu_2$  vibrational band. The remainder could not be assigned with certainty, but presumably involved higher rotational and/or vibrational excitation. Simultaneously Oka published<sup>17</sup> 15 vibration-rotational transition frequencies in  $\text{H}_3^+$  to an accuracy of 2 ppm, using laser infrared difference-frequency spectroscopy of a cooled hydrogen discharge. The transitions were successfully assigned by Watson.<sup>17</sup> Subsequently in 1981 we observed<sup>18,19</sup> the spectra of  $\text{H}_2\text{D}^+$  and  $\text{HD}_2^+$ , also measured additional transitions in  $\text{D}_3^+$ .

## B. Importance

Historically, stable atoms and molecules containing one or two electrons were crucial to the development of modern quantum theory, since only they are simple enough in structure to permit highly precise comparisons of the predictions of theory with the results of experiment. The triatomic hydrogen molecular ion is the simplest well-bound polyatomic system. It consists of three nuclei and two electrons, it plays a role in the chemistry of polyatomic species analogous to that of  $\text{H}_2^+$  or  $\text{H}_2$  in the chemistry of diatomic ions or molecules.

Molecular ions also play an important role in the chemistry of dense molecular clouds in the interstellar medium,<sup>20,21</sup> which are believed to be the site of protostar formation. It appears from detailed computer models of cloud chemistry that the observed abundances of simple interstellar molecules can be reproduced by sequences of ion-molecule reactions.<sup>22</sup>

Because of the high stability of  $\text{H}_3^+$  and its high production cross section via reaction (1) ( $\sim 100 \text{ \AA}^2$  at room temperature, and  $\sim 500 \text{ \AA}^2$  in interstellar medium), the  $\text{H}_3^+$  isotopes, rather than the  $\text{H}_2^+$  isotopes, are the dominant hydrogenic molecular ions both in a hydrogen discharge and



in molecular clouds. The  $\text{H}_3^+$  ion plays a crucial role acts as an efficient proton or deuteron donor<sup>23</sup> in chemical reactions which are responsible for the productions of protonated or deuterated molecules in the interstellar medium.

At first glance, it might seem that  $\text{H}_2\text{D}^+$  would be much less abundant than  $\text{H}_3^+$  because the cosmic  $[\text{D}]/[\text{H}]$  abundance ratio is approximately  $2 \times 10^{-5}$ . However, it is widely accepted that pronounced isotopic fractionation can occur in the interstellar medium, based on the different zero-point energies for H- and D-containing molecules. Hence,  $[\text{D}]/[\text{H}]$  abundance ratios in specific molecules differ dramatically (by some four or five orders of magnitude in the case of the  $[\text{DCO}^+]/[\text{HCO}^+]$  ratio<sup>24,25</sup>) from the cosmic abundance ratio.  $\text{H}_2\text{D}^+$ , which is produced mainly by the reaction,<sup>21</sup>



in dense interstellar clouds, is believed to be the major intermediate species in the chain of fractionation reactions, and is probably present in substantial quantities. Despite the presumed large abundances of  $\text{H}_3^+$  and  $\text{H}_2\text{D}^+$  in the interstellar clouds, they have not yet been observed in the interstellar medium.<sup>26,27</sup>

Apart from its intrinsic interest, isotopic fractionation is important as a systematic correction which must be applied to the  $[\text{D}]/[\text{H}]$  abundances observed in molecules in order to obtain the true cosmic  $[\text{D}]/[\text{H}]$  isotopic abundance ratio. Models of interstellar clouds are strongly dependent on the assumed cosmic abundance ratio.<sup>20,28</sup> The cosmic  $[\text{D}]/[\text{H}]$  abundance presumably partially reflects the isotopic abundance produced in big-bang nucleosynthesis, and hence has cosmological significance.

Finally, it has also been suggested that  $\text{H}_3^+$  might be important in Jovian atmospheric chemistry<sup>29</sup> and might have an effect on thermodynamic behaviors of some metallic hydrides.<sup>30</sup>

## II. Experiments of the Structure of $\text{H}_3^+$

In this section, we briefly describe other experimental results on the structure of  $\text{H}_3^+$ . Our experimental method and results will be presented in detail in following sections.

### A. Beam-foil-induced dissociation

The first experimental determinations of the geometry of the  $\text{H}_3^+$  ion were carried out by three different groups (Argonne, Lyon, and Rehovot) in 1978<sup>12</sup>. They took  $\text{H}_3^+$  ion beams of a few MeV, used them to bombard a target foil ( $\sim 100$  Å of carbon), and looked at the dissociation fragments that emerged after the foil. As the high-speed molecular ion bom-

bards the target, its binding electrons are stripped off within a few angstroms after penetrating the front surface of the foil. That leaves a light cluster of atomic ions (protons for  $\text{H}_3^+$ ) that remain correlated in space and time as they progress through the foil. The ions repel each other apart in a "Coulomb explosion", dumping their initial potential energy into center-of-mass kinetic energy. So emerging from the foil, one has fragments with both the original beam velocity and a component from the Coulomb explosion. This component causes a shift in the laboratory energy and angle of each fragment; the shift depends on the orientation of the incoming molecular ion. Therefore, analysis of the fragments emerging from the foil reveals information about the geometrical structure of the molecular ion.

All three experiments revealed an equilateral triangular structure for  $\text{H}_3^+$  with a bond distance of  $0.97 \pm 0.03$  Å. The experimental bond distance is larger than theoretical value (0.873 Å). This is due to the incident molecular ions being populated in a range of vibrationally excited states. A theoretical analysis<sup>31</sup> of the bond distance distribution with the vibrational population calculated by Smith and Futrell<sup>32</sup> agrees with experimental values quite well.

#### B. Rydberg state emission spectra of neutral $\text{H}_3$ and $\text{D}_3$

$\text{H}_3$  is not a stable polyatomic molecule in its ground state; however, its Rydberg states can be stable bound states since the core,  $\text{H}_3^+$ , is stable. The transitions between  $\text{H}_3$  (and  $\text{D}_3$ ) Rydberg states were first observed in an ordinary hollow cathode discharge tube through  $\text{H}_2$  or  $\text{D}_2$  by G. Herzberg in 1979.<sup>13,33</sup> The  $\text{H}_3$  (or  $\text{D}_3$ ) molecules are formed by ion-electron recombination in the hydrogen discharge plasma, in which the  $\text{H}_3^+$  (or  $\text{D}_3^+$ ) is the most abundant ion. Since adding a loosely bound electron to the highly stable  $\text{H}_3^+$  core will not change the molecular geometry much, the analysis of the Rydberg spectra of  $\text{H}_3$  and  $\text{D}_3$  will indirectly reveal the structure of  $\text{H}_3^+$  or  $\text{D}_3^+$ . A comparison between the rotational constants of  $\text{H}_3$ ,  $\text{D}_3$ , and corresponding core ions,  $\text{H}_3^+$ ,  $\text{D}_3^+$ , manifests this fact. More recently, Figger et al.<sup>34</sup> have observed and assigned some new transitions of  $\text{D}_3$  by monitoring the laser-induced charge of the emission from selected levels of  $\text{D}_3$ .

#### C. Infrared spectrum of $\text{H}_3^+$

The infrared  $\nu_2$  band of  $\text{H}_3^+$  was observed by T. Oka in 1981.<sup>17</sup> A direct infrared absorption method combining a liquid-nitrogen-cooled multiple-reflection discharge cell<sup>35</sup> and a difference-frequency infrared radiation source<sup>36</sup> was used for this observation. A continuous scan of the region between  $2800$ – $2460$   $\text{cm}^{-1}$  produced nine transitions assigned to  $\text{H}_3^+$ , which were predicted by Watson using the rotational constants from the ab initio results of Carney and Porter.<sup>11</sup> Subsequently, six more transitions were observed close to their predicted positions. Later,



Oka<sup>37</sup> found 15 more lines originated from higher rotational states by cooling the discharge with ice water. The observed linewidth was about 0.01  $\text{cm}^{-1}$  (or 300 MHz) and the accuracy of the measurements is about 0.005  $\text{cm}^{-1}$  (or 150 MHz).

#### D. Infrared spectrum of $\text{H}_3^+$ , $\text{D}_2\text{H}^+$ and $\text{D}_3^+$ at dissociation limit

Recently, A. Carrington <sup>38</sup> et al. observed the infrared spectrum @ $\sim 10$   $\mu\text{m}$  of  $\text{H}_3^+$  at the dissociation limit. The spectrum arises from transitions between bound levels lying below the  $\text{H}_2 + \text{H}^+$  dissociation limit and metastable levels lying above. The existence of metastable levels is due to the centrifugal energy barrier arising from rotation of the  $\text{H}_3^+$  molecule. Our experimental method was used by them in this observation. A  $\text{CO}_2$  laser was used to induce the transitions which were detected by monitoring the  $\text{H}^+$  ions formed through rotational predissociation.  $\text{H}_3^+$  ions are formed in an electron impact ionization source. So far they have recorded more than 300 lines (with a density of 100 lines/ $\text{cm}^{-1}$ ), and believe that the total spectrum accessible to them might well contain over 30,000 lines (over 230  $\text{cm}^{-1}$  frequency range). No resonance lines were observed when the electron impact source was replaced by a plasmatron ion source operated at source pressures two to three orders of magnitude higher. This shows that vibration-rotational levels near dissociation limit are populated by the ion-molecule reaction, and are depopulated by collisions occurring in the plasmatron source. The interpretation of the observed spectrum will be quite different from the vibration-rotation spectra for  $\text{H}_3^+$  and  $\text{D}_3^+$  in their lowest vibrational states. At the present time, very little appropriate theory exists. It seems likely that the complexity of the observed spectrum arises from a breakdown of some of the normal vibration-rotation selection rules, as well as from a high density of levels (near the dissociation limit).

In addition to  $\text{H}_3^+$ , they have observed similar spectra for  $\text{D}_2\text{H}^+$  and  $\text{D}_3^+$ . For  $\text{D}_2\text{H}^+$  there are two possible modes of photodissociation, to either  $\text{D}_2 + \text{H}^+$  or  $\text{HD} + \text{D}^+$ . The spectrum of  $\text{D}_2\text{H}^+$  could be observed only by detecting  $\text{H}^+$  ions, but not  $\text{D}^+$  ions. This can be explained by the fact that the  $\text{D}_2(\text{v}=0) + \text{H}^+$  dissociation limit is lower than the  $\text{HD}(\text{v}=0) + \text{D}^+$  limit by 372  $\text{cm}^{-1}$ , mainly because of the difference in zero point energies between  $\text{D}_2$  and  $\text{HD}$ . The spectrum of  $\text{D}_3^+$  was considerably weaker than that of  $\text{H}_3^+$ , presumably because of the higher density of vibration-rotation levels and consequently lower populations.

### III. Apparatus and Procedures

In obtaining the present results the Doppler-tuned fast-ion-beam laser-spectroscopic method was used; a schematic diagram of the physical apparatus involved in our measurement is given in Fig. 1. A beam of molecular ions is crossed by a nearly collinear cw fixed-frequency CO

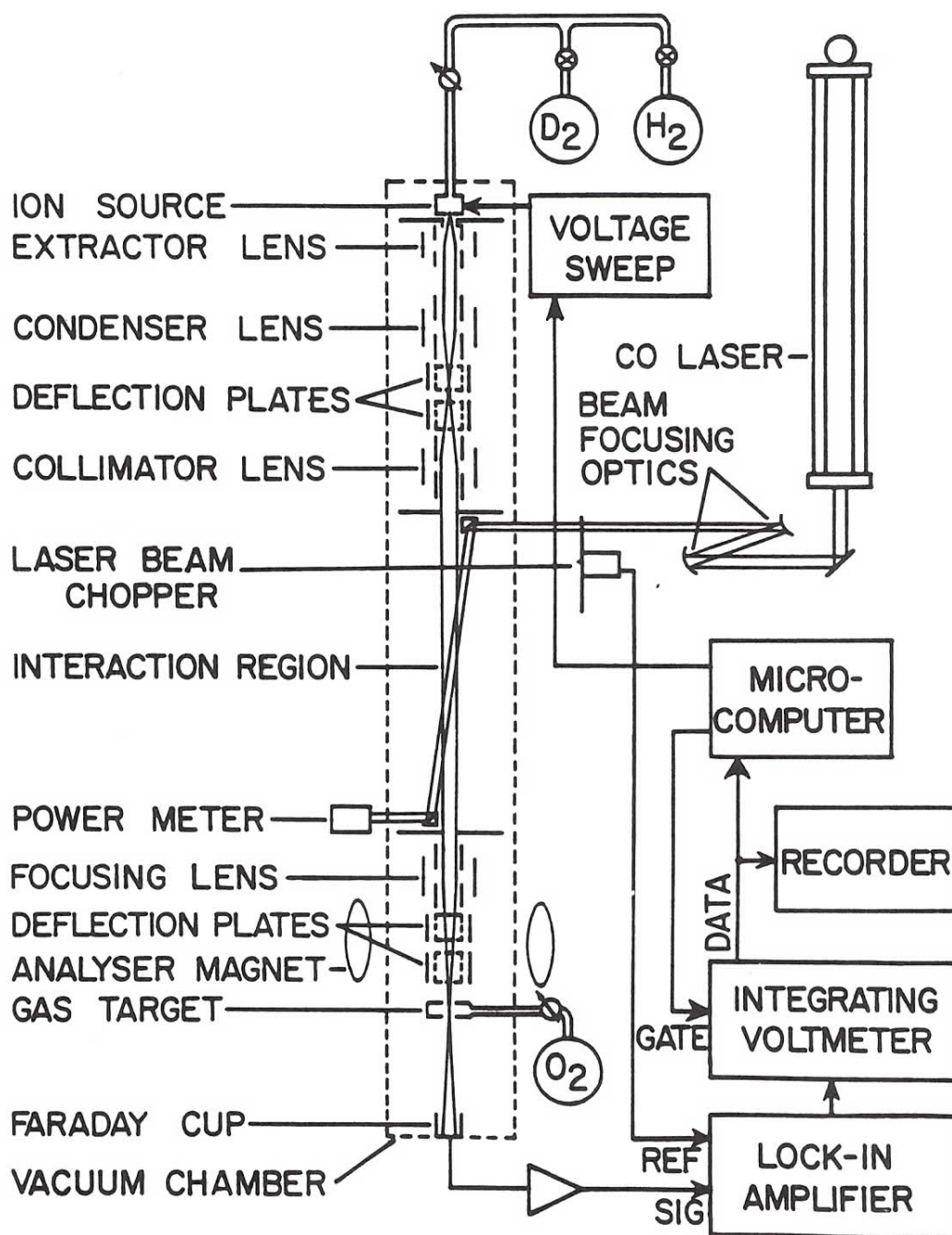


FIG.1 Doppler tuned ion beam laser resonance method schematic.  
 -- The laser beam direction can be reversed so that it is nearly anti-parallel to the ion beam. Not shown are two long-coil pairs which cancel transverse components of the laboratory magnetic field.



laser beam. The CO line frequency is Doppler tuned into resonance with a nearby transition by sweeping the beam-accelerating voltage. After interaction with the CO laser beam, the ions are partially charge-exchange neutralized by collision with gas in a target chamber. A resonance is observed as a modulation in the surviving ion beam current upon chopping the laser beam at 1 kHz frequency. This apparatus can be considered as an optical-frequency analogue of a molecular-beam electric-resonance spectrometer. The principles of the method<sup>39</sup> and the construction and operation of the ion source<sup>40,41</sup> have been described elsewhere. Features particular to the present studies will be discussed here.

#### A. Ion source and population distributions

A cross-sectional view of the source is shown in Fig. 2. Electrons are emitted thermally from the concave spherical dispenser cathode, and are then accelerated and focused into the ionization/reaction channel. A mixture of  $H_2$  and  $D_2$  is fed into the ionization/reaction channel through radial inlets after purification by a hot palladium leak. We used  $D_2$  for the  $D_3^+$  study and a mixture of  $H_2$  and  $D_2$  for the  $H_2D^+$  and  $HD_2^+$  study ( $H_2 : D_2 = 65\%:35\%$  and  $35\%:65\%$  for  $H_2D^+$  and  $HD_2^+$ , respectively). The palladium leak breaks hydrogen molecules into atoms which then randomly recombine into molecules after they diffuse through the palladium leak; therefore, the gas going into the ion source for the study of  $H_2D^+$  and  $HD_2^+$  will contain HD as well as  $H_2$  and  $D_2$ .

The production mechanism of  $H_3^+$  isotopes is electron-impact ionization of  $H_2$  isotopes followed by reaction with  $H_2$  isotopes. The principal destruction reaction for  $H_3^+$  isotopes is collisional dissociation with  $H_2$  isotopes and dissociative recombination with electrons.

The  $H_3^+$  isotopes produced by ion-molecule reactions are vibrationally excited, due to the large energy difference ( $\sim 1.7$  eV) between the reactants and the products. A statistical model<sup>32</sup> which assumes a random distribution of energy among the vibrational and translational states of the products of reaction (1) shows a broad distribution of energy states of  $H_3^+$  and  $D_3^+$ . A definite probability exists for ions to have energies from zero up to nearly dissociation limit. Several experiments<sup>32,42-44</sup> in addition to the observation of the IR transitions in  $H_3^+$  isotopes at their dissociation limit<sup>38</sup> support this assertion. Those experiments also showed the collisions of the excited  $H_3^+$  (or  $D_3^+$ ) with  $H_2$  ( $D_2$ ) rapidly deactivate the vibrational excitation. Leventhal and Friedman<sup>42</sup> concluded that the vibrational energy is de-excited in 1 to 4 collisions, while Smith and Futrell<sup>32</sup> concluded that complete deactivation appears to occur after 5 to 10 collisions. Some authors<sup>45-47</sup> have noticed "ion source effects" in their  $H_3^+$  collision experiments, presumably owing to changes in vibrational excitation caused by changes in the ion source pressure. In fact, Peart and Dolder produced a beam of  $H_3^+$  ions in the ground vibrational state by operating the ion source at pressure higher than 0.1

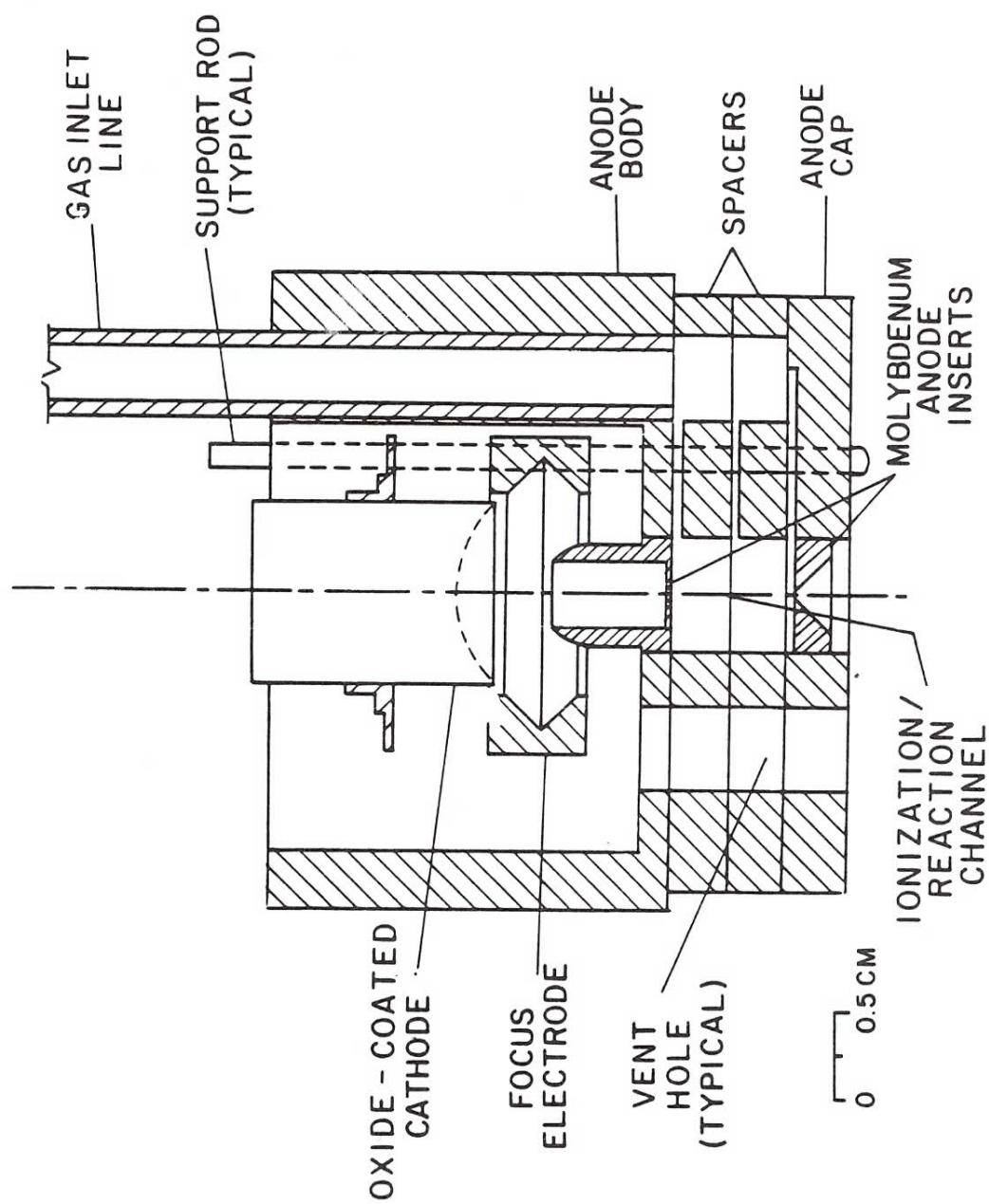


FIG. 2 Ion source schematic. -- The left half-section is rotated  $22.5^\circ$  from the right half to show vent hole detail. From Ref. (83).

Torr<sup>48</sup>. The normal operating pressure for our source (0.6 Torr) is several times higher than theirs; we believe that the dominant ions in the  $H_3^+$  beam produced by our source are in the ground vibrational state.

As far as rotational temperature is concerned, we have not found any theoretical or experimental studies in the literature. The rotational temperature could be much higher than the source temperature ( $\approx 350^\circ K$ ), or the population distribution could be extremely non-thermal.

#### B. Doppler tuning

The desired ions are extracted from the source along with many other ions, e.g.,  $D_2^+$  and  $D^+$  with  $D_3^+$ , and then are accelerated and focussed to form a beam of a few keV energy, which is intercepted at a small angle (10.825 mrad) in a field-free space by a laser beam from a fixed-frequency infrared CO laser. The accelerating voltage of the ion beam is swept in order to Doppler-shift a vibrational-rotational transition in the desired molecular ions into resonance with the laser beam. The Doppler-shifted laser frequency  $f'$ , seen by ions in the beam, is given by

$$f' = f \left( \frac{1 - \beta \cos \theta}{\sqrt{1 - \beta^2}} \right) \quad (3)$$

where  $\beta = u/c$  and  $u$  is the speed of the molecular ion,  $\theta$  is the laboratory angle between the ion velocity and the laser beam direction, and  $f$  is the laser frequency in the laboratory frame.

Fast ion-beam spectroscopy has the ability to obtain sub-Doppler resolution due to the narrowing of the velocity distribution in an ion beam when it is accelerated, or "kinematic compression".<sup>49</sup> This arises very simply from the fact that a population of ions with an energy spread  $\Delta E$  that is extracted from an ion source and accelerated to an energy  $E$  maintains this energy spread  $\Delta E$ ; however, since  $E \approx mv^2/2$ , the velocity spread at an energy  $E \gg \Delta E$  is substantially reduced from its value before acceleration. It is easy to show that the velocity spread is reduced by a factor<sup>49</sup>

$$B \approx \frac{1}{2} \sqrt{\frac{\Delta E}{E}} \quad (4)$$

and then, the translational temperature is reduced by a factor of

$$C \approx \frac{1}{4} \sqrt{\frac{\Delta E}{E}} \quad (5)$$

where  $\Delta E$  is the kinetic energy spread of the ion beam. For example, an ion beam with a 1 eV energy spread has at 3 keV laboratory energy a



velocity spread similar to a temperature of about 1°K. However, acceleration does not cool the vibrational and rotational temperatures.

### C. CO laser

We use a stable cw sealed-off  $^{12}\text{C}^{16}\text{O}$  laser built according to the design of Freed<sup>50</sup>. The cavity consists of a PZT-mounted coupling mirror having 3-m radius at one end and a line-selective diffraction grating at the other end. This laser will be designated as a LS (line selective) laser. The cavity length is 1.5 meters. The gain medium is a 115-cm-long discharge cooled to between -30 to -50°C. The laser is filled with a mixture of 13.4%  $\text{N}_2$ , 3.2%  $\text{CO}$ , 8.1%  $\text{Xe}$ , and 75.3%  $\text{He}$  at 18.6 Torr. The cathode is cooled by compressed air. The gain profile width of each line ( $\sim 120$  MHz) is slightly larger than the spacing (100 MHz) between two longitudinal modes. The laser is capable of operating on over one hundred lines in the range 5.1-6.4  $\mu\text{m}$  (or 1550-1975  $\text{cm}^{-1}$ ). Power in an individual line ranges from a few mW up to more than 1 W.

There are usually two, or occasionally three, CO molecular lines lasing at a given grating position. In order to lock the laser at the center of a particular line (thereby reducing the laser frequency), a filter is needed to select the line to be locked. In the experiment, a small part of the laser output is beam-split into a scanning Fabry-Perot, and the filtered laser line is monitored by a thermoelectrically cooled PbSe detector. Two feedback loops were employed for active locking; one of the loops locked a transmission maximum of the scanning Fabry-Perot to the line we wanted to lock and the other loop locked the laser to the maximum or minimum of the power of this line.

Locking the laser cavity length to the maximum of the filtered line corresponds to locking at its center frequency and lasing occurs on one longitudinal mode (called one-mode locking later). Locking to the minimum corresponds to lasing on two longitudinal modes at equal distance from the center (called two-mode locking later). Due to the sharper gain profile (typically 3-5 MHz, instead of 100 MHz) for two-mode locking, the latter gave us better stability ( $\lesssim 100$  kHz) than the former. We usually employed the two-mode locking for final precision measurement of molecular intervals. Until 1981 the locking was done by two phase-sensitive detectors with laser cavity and Fabry-Perot lengths dithered at different frequencies with small amplitudes. Currently, we use a microcomputer to do the locking, which does not need to dither the laser cavity and Fabry-Perot lengths; it therefore reduces the laser linewidth compared to the analog method. The digital locking also has a higher success rate than the analog locking. The details of the analog and digital locking will be published elsewhere.<sup>51</sup>

### D. Choice of target gas

Observation of the resonances with such a high-resolution technique



as we have used entailed serious search problems in view of the large uncertainty attached to the theoretical estimates. Our apparatus can search approximately  $1\text{--}2\text{ cm}^{-1}$  per day, whereas the uncertainty in the best theoretical estimates<sup>10</sup> was approximately an order of magnitude greater. In our previous work on  $^4\text{HeH}^+$ <sup>16</sup>, we were able to use the position of the early resonances discovered to guide our search for the later ones. This process, made possible by unambiguous identification of the transitions based on *ab initio* calculation, converged rapidly. In the present study, this convergence procedure cannot be employed until a large number of resonances have been observed, because the higher density of energy levels and less complete state of the existing theoretical calculations makes transition identification difficult. Therefore, increasing search speed by optimizing SNR is very important.

After interaction with the laser beam, the desired ions are mass-selected by crossed electric and magnetic fields, and pass through a gas target and suffer attenuation by a variety of collisional mechanisms. The surviving fraction is collected in a Faraday cup. The main attenuation mechanism of  $\text{H}_3^+$  isotopes in the few-keV range is charge-exchange neutralization followed by dissociation into neutral fragments. The cross sections for such collision processes commonly differ by a few percent among vibrational states. The previously mentioned "ion source effects" in  $\text{H}_3^+$  collision experiments<sup>45-47</sup> manifest this. If the resonating states differ in initial populations, the laser-induced transition will produce a net population transfer. Consequently, the laser resonance changes the beam-charge survival in the gas target and, hence, the current collected at the Faraday cup.

The efficiency of the collision detection depends on the target gas used. The larger the difference between the cross sections for the two levels connected by the transition is the larger the signal will be. Therefore, one way to increase the efficiency is to experiment with different target gases and pick the one that gives the strongest signal. Also, the initial choice of target gas is important in that is you use a target gas which gives you zero difference in the cross section, e.g.,  $\text{N}_2$  for this work (see later), you will never find any transitions.

For the present study, we chose Ar to start looking for resonances. Experiments<sup>46</sup> have shown that the charge exchange and dissociation cross sections for  $\text{H}_3^+$  ions of 2- to 50-keV energy incident upon Ar are larger compared to  $\text{H}_2$  and other inert gases (He, Ne). We began to search for  $\text{D}_3^+$  transitions around  $1760\text{ cm}^{-1}$  with Ar target gas set such that the  $\text{D}_3^+$  beam was attenuated to 75% level. After a 24-hour search, we saw the first transition.

Fixing the source conditions (this defines the population distribution), we optimized the signal strength by varying the attenuation. Then, we did the same experiment for other common gases. We have tried the

following gases: Ar, He, H<sub>2</sub>, N<sub>2</sub>, CO, CO<sub>2</sub>, O<sub>2</sub>, C<sub>4</sub>H<sub>6</sub>, CH<sub>3</sub>CO, and C<sub>2</sub>H<sub>5</sub>OH. The relative optimized signal sizes are listed in Table 1. One may notice that the He gives you an opposite signal compared to other gases, and N<sub>2</sub> gives you a zero signal. Also, for all target gases (except He), the signal at resonance corresponds to a decrease of beam current.

The final choice of target gas is oxygen. The reason that we did not use ethanol (C<sub>2</sub>H<sub>5</sub>OH), even though it gave the largest signal, is that the attenuation of beam current is not stable, which could be due to its high vapor pressure at room temperature and concomitant tendency to condense in the apparatus.

Then, we tried to maximize the signal-to-noise ratio by adjusting the ion source pressure. In the actual experiment, we always optimized the beam current of the specific ion under study by adjusting the ion source conditions at the optimized source pressure.

#### E. Multiplicity advantage

We further increased the searching speed by operating the spectrometer in a new fast-scan mode in addition to the traditional slow-scan mode. In the fast-scan mode, the line-selective grating in the LS CO laser was replaced by an infrared mirror, causing laser oscillation on approximately 15 molecular CO lines. We will call this laser an NLS (non-line-

Table 1 Relative optimized signal strength for various target gases

Target gas	Optimized signal w.r.t. O <sub>2</sub> <sup>a</sup>
O <sub>2</sub>	1.0
C <sub>4</sub> H <sub>6</sub> (1,3-Butadien)	0.9
CH <sub>3</sub> OH (Methanol)	0.9
CH <sub>3</sub> CO (Acetone)	0.9
C <sub>2</sub> H <sub>5</sub> OH (Ethanol)	1.1
N <sub>2</sub>	0.0
H <sub>2</sub>	0.7
CO <sub>2</sub>	0.5
CO	0.5
Ar	0.3
He <sup>b</sup>	-0.4

<sup>a</sup>The signal at resonance with O<sub>2</sub> target corresponds to decrease in the beam current.

<sup>b</sup>This is not the optimized signal strength for He. The limit of foreline pressure (200 μm Hg) did not allow us to increase the He pressure to the optimized value.



selective) laser later. The spectrometer thereby achieved a "multiplex advantage", scanning 15 segments of the spectrum simultaneously and reducing the mean search time between resonances by about the same factor. Our resonance search procedure consisted of two stages. First, the spectrometer was operated in the fast-scan mode using LS laser to find the resonances. This step determines the resonance beam voltage but does not identify the particular CO laser line driving the transition. Second, the spectrometer was operated in the slow-scan mode using LS laser to identify the individual CO laser line.

The power output of the NLS laser is roughly 4.5 W at  $-40^{\circ}\text{C}$ . It tends to lase on 15-20 lines in a cascade scheme<sup>52</sup>, and the spectral distribution has a sensitive dependence on the cavity length. The laser cavity length can be stabilized by locking it to the peak power of one of the stronger lines, using the method described previously for LS laser.

We analyzed the spectral content of the NLS laser output by directing the laser beam into a monochromator after it interacted with the ion beam. A thermoelectrically-cooled PbSe detector and phase sensitive detector (using the same chopper reference used for signal detection) were used to detect the laser beam through the monochromator. In this way, we knew which laser lines were operating while we searched for resonances.

#### IV. Data Analysis and Experimental Results

##### A. $\text{D}_3^+$

As mentioned before, there are usually two or three CO lines lasing at a grating position with LS laser. After each resonance voltage was detected, we had to identify the CO line which drove the resonance. Two methods were used to identify the driving CO line. One was to successively set the grating at a pre-calibrated position for each line, lock it on 2 longitudinal modes, and scan around the resonance voltage to see whether or not another copy of the resonance (displaced by laser mode spacing of 100 MHz) was present. In order to assure the calibration, we checked the laser wavelengths with the monochromator occasionally. The other way was to detect the same transition with a second laser line at different beam voltage. Usually, the second method was used in the identification of the laser line.

After the laser line was identified, a more careful scan was made to acquire data for measurement. For these scans, the beam line was carefully optimized and the stray laboratory magnetic field in the interaction region was carefully zeroed. Most final scans were done with a step size of 0.125 or 0.25 volts and integration time of 4 to 64 secs, depending on the strength of the resonances. In most final scans, the laser line was two-mode locked to assure the highest accuracy and stability. For the cases in which the laser could not be two-mode locked, it was one-mode

locked. A typical resonance signal is shown in Fig. 3. The typical signal-to-noise ratio was about 15 in a total integration time of 10 minutes.

The Fig. 3 displays a slight asymmetry, being skewed out on the high voltage side. All the resonances observed exhibited this behavior to some degree. Apparently this is not due to hyperfine splittings, however, since the observed asymmetries are always on the higher voltage side of the resonance, regardless of whether the laser is directed parallel to (Doppler down-shifted) or antiparallel to (Doppler up-shifted) the ion beam. Such a situation probably arises from an asymmetrical distribution of initial ion velocities.

The output of the experiment is a chart recorder trace. The beam voltages at the beginning and at the end of the run were measured and recorded, providing an accurate voltage calibration for the trace. Some experimental outputs were also recorded on floppy disks for later analysis. The center voltage could be determined to within  $\pm 0.15$  volts "by eye". This uncertainty has been verified by a BASIC program which finds the centroid of the resonance.

Some careful scans show that there is a weak resonance peak nearby one resonance peak when the laser is locked at two-mode. The peak is due to the second transverse ( $TEM_{10}$ ) mode. The CO laser has limiting apertures to suppress the higher transverse modes; however, it can still lase at  $TEM_{10}$  mode when the gain is high. An average of six scans yields a separation of  $22 \pm 2$  MHz between  $TEM_{00}$  and  $TEM_{10}$  which agrees very well with the value (25 MHz) estimated by the following equation<sup>53</sup>

$$\Delta\nu = \frac{c}{2\pi\ell} \left( \tan^{-1} \frac{z_2}{z_0} - \tan^{-1} \frac{z_1}{z_0} \right), \quad (6)$$

for our laser cavity  $z_2 = z_0 = 150$  cm and  $z_1 = 0$ .

There are effects which can cause the ions to have an energy different from the measured beam voltages. Examples might be a potential difference at plasma boundary in the ion source, space-charge-induced potentials both in the ion source and in the ion beam itself, and kinetic energy of ions produced by ion-molecule reaction.<sup>54</sup> The potential offset can be studied by observing several transitions each with several different laser lines, and adjusting a hypothesized contact potential offset to obtain consistency.

For simplicity, we assume that the potential offset is a constant plus a small voltage dependent contribution which was subsequently found to be negligible. Seven pairs of measurements, each consisting of measurements at parallel and antiparallel beam directions of the same transition with two different laser lines, are used in the present analysis. Two



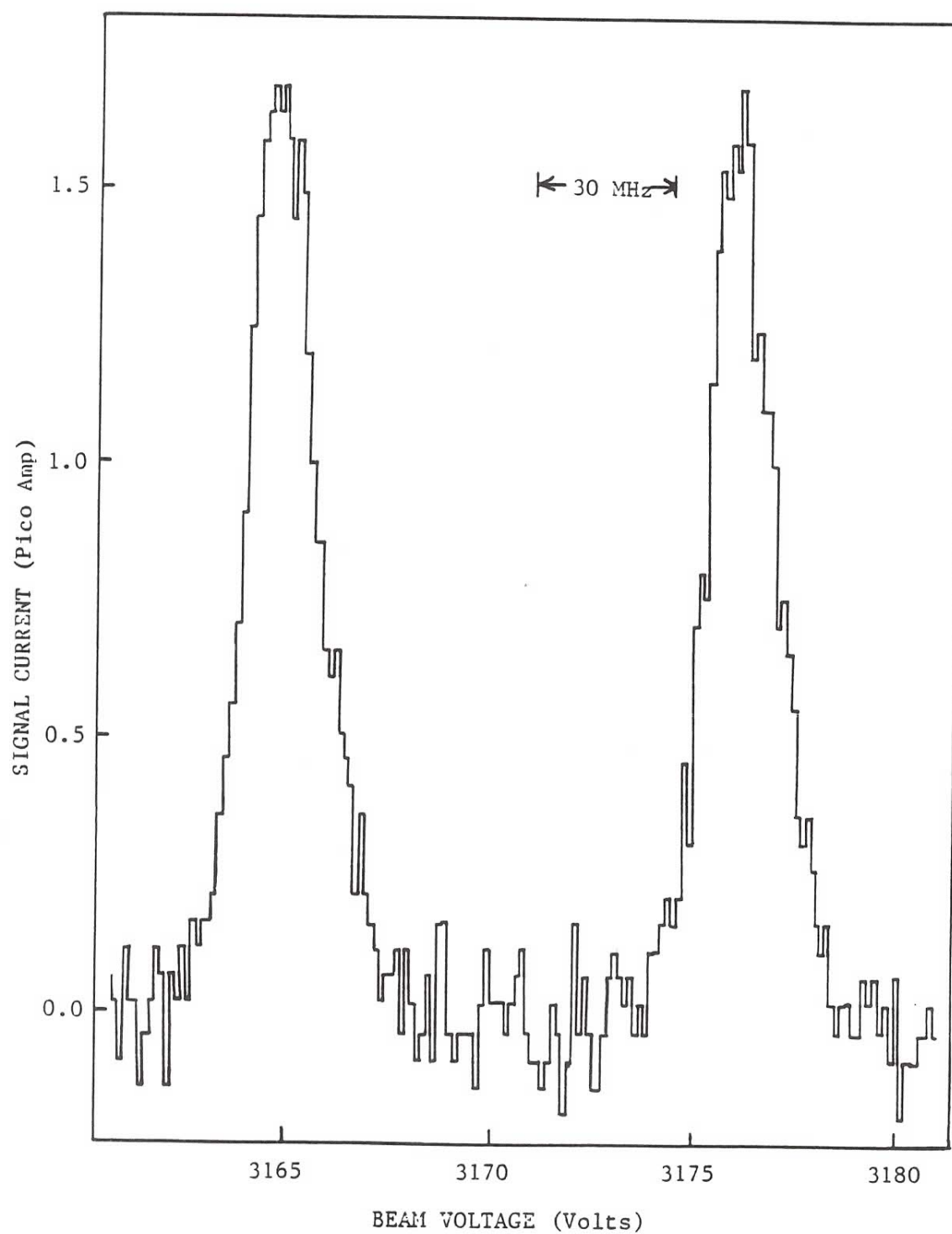


Fig. 3. Chart recorder trace of No. 1  $D_3^+$  transition. -- The resonance trace shows two peaks separated by the laser free-spectral range of 100 MHz due to two mode locking. Ref. to TABLE 5 - for numbering of the transitions.

TABLE 2 Summary of the study of potential offset for  $D_3^+$ .

$^{12}C^{16}O$ -Laser transition		$D_3^+$ Ion transition				
( $v', N'$ )-( $v'', N''$ )	Assumed <sup>a</sup> frequency ( $cm^{-1}$ )	Measured <sup>b</sup> resonance voltage (V)	Uncorrected <sup>c</sup> frequency ( $cm^{-1}$ )	Potential offset (V)	Corrected <sup>b,d</sup> resonance voltage (V)	Corrected frequency ( $cm^{-1}$ )
(11,12)-(10,13)	1833.5262	-4251.25	1831.2741	+1.72	-4253.10	1831.2736
(11,13)-(10,14)	1829.5899	+2379.50	1831.2730		+2381.35	1831.2737
(9,20)-(8,21)	1851.3842	-3137.35	1849.4305	+2.05	-3139.20	1849.4299
(10,15)-(9,16)	1846.8855	+5331.75	1849.4293		+5333.60	1849.4298
(9,20)-(8,21)	1851.3842	-3137.35	1849.4305	+1.74	-3139.20	1849.4299
(9,21)-(8,22)	1847.1185	+4399.70	1849.4295		+4401.55	1849.4300
(10,13)-(9,14)	1854.9269	-4061.10	1852.7000	+2.01	-4062.95	1852.6995
(10,14)-(9,15)	1850.9226	+2589.00	1852.6987		+2590.85	1852.6994
(9,17)-(8,18)	1863.9893	-3216.95	1861.9975	+1.91	-3218.80	1861.9969
(10,12)-(9,13)	1858.8982	+7805.20	1861.9965		+7807.05	1861.9969
(9,17)-(8,13)	1863.9893	-3216.95	1861.9975	+1.75	-3218.80	1861.9969
(9,18)-(8,19)	1859.8198	+3850.30	1861.9964		+3852.15	1861.9970
Average				+1.86±0.13		

<sup>a</sup>Taken from Ref. 56. The assigned uncertainty was  $\pm 0.0001 \text{ cm}^{-1}$ .<sup>b</sup>Beam direction is parallel for negative voltages and is anti-parallel for positive voltages.<sup>c</sup>Frequency calculated from measured resonance voltage.<sup>d</sup>The least-squares fit result is used here (see text).

methods are used to determine this constant potential offset. The offset voltage for each pair of measurements is determined and averaged in the first (or averaging) method, which gives an offset of  $+1.86 \pm 0.13$  volts. In the second method, a constant offset is added to all the measured voltages and the square of the difference between measurements of each pair are minimized by adjusting this constant offset. This least-squares fitting method gives us an offset of  $+1.85 \pm 0.13$  volts, which agrees very well with the averaging method. The small uncertainty ( $\pm 0.13$  volts) in the results verifies the assumption of constant offset at the beginning. The results are shown in Table 2; and the agreements between different measurements on the same transition are under  $0.0001 \text{ cm}^{-1}$  after applying this offset.

The  $+1.85$  volts offset is then applied to four other pairs of measurements, listed in Table 3. Three of those four pairs consist of two

TABLE 3 List of measurements not used in  $D_3^+$  potential offset study.

$^{12}\text{C}^{16}\text{O}$ -Laser transition		$D_3^+$ Ion transition			
$(v', N') - (v'', N'')$	Assumed frequency ( $\text{cm}^{-1}$ )	Measured resonance voltage (V)	Uncorrected frequency ( $\text{cm}^{-1}$ )	Corrected resonance voltage (V)	Corrected frequency ( $\text{cm}^{-1}$ )
(10,22)-( 9,23)	1817.7208	+2698.40	1819.5012	+2700.25	1819.5022
(11,16)-(10,17)	1817.5840	+3128.45	1819.5014	+3130.30	1819.5019
(10,21)-( 9,22) <sup>a</sup>	1821.9831	-4043.25	1819.8005	-4045.10	1819.8000
(11,15)-(10,16) <sup>a</sup>	1821.6186	-2805.25	1819.8008	-2807.10	1819.8002
(10,17)-( 9,18) <sup>a</sup>	1838.7137	-3624.20	1836.6283	-3626.05	1836.6278 <sup>b</sup>
(10,18)-( 9,19)	1834.5792	+3499.90	1836.6262	+3501.75	1836.6268
(10,15)-( 9,16) <sup>a</sup>	1846.8855	-5998.00	1844.1912	-5999.85	1844.1908
( 9,21)-( 8,22) <sup>a</sup>	1847.1185	-7079.80	1844.1911	-7081.65	1844.1908

<sup>a</sup>Laser locked at single mode

<sup>b</sup>Not used in final result (see text).

measurements on the same transition at the same beam direction. Since the difference between two measurements done at the same beam direction is small, due to the same sign of Doppler shift, they are not used in the present analysis. The only pair left consists of two measurements on the same transition at both beam directions; however, it is also excluded



from the analysis. For this transition, one of the laser lines (10,17)-(9,18) used in the measurement has a nearby absorption line which is (15,20)-(14,19) CO molecular line at frequency 40 MHz higher. Therefore, the gain profile for (10,17)-(9,18) is higher at the lower frequency side and its peak is moved to the lower frequency side of the line center. The single-mode locking, which locks the laser to the peak of its gain profile, will give us lower laser frequency than the center. Since the position of the peak of the gain profile depends on laser operation conditions, the measurement done with this line will not be used in the final transition frequency measurement. However, the discrepancy of the two measurements will be reduced if we take this into account. This nearby absorption is also responsible for the unstability of the two-mode operation, i.e., the laser would not run two modes simultaneously at this molecular line even if its gain is high enough.

We have done several careful scans for two transitions at different ion source pressures. The purpose is to check any dependence of resonance voltage, linewidth, and signal strength on source pressure. The dependence of the signal strength on source pressure may also be useful for identification of the transition. This dependence on source pressure may be different for high and low rotational levels, if the rotational population distribution is nonthermal.

It is found that the measured resonance voltages increase roughly linearly with source pressure, while the linewidths are approximately the same over the whole range of pressure. This effect, combining the result of the last section, presents an interesting situation: the "true" resonance voltage could not be obtained by extrapolating the measured resonance voltage to zero ion source pressure. In this case the constant potential offset at zero source pressure is 2.05 volts. The measured resonance voltages are fitted to a linear function of source pressure, as shown in Table 4, which gives a slope of 0.08 volts per  $\times 10^{-5}$  Torr source chamber pressure. All the careful runs were taken at roughly the same source pressure ( $2.5 \pm 0.3 \times 10^{-5}$  Torr); and thus the voltage offset calculated in the previous section includes this effect; only a negligible ( $\pm 0.03$  V) uncertainty would result from the range of pressures used.

The experimentally observed transition frequencies are presented in Table 5 (eight of them have been published before<sup>14</sup>), along with the CO laser frequencies, corrected resonance voltages, linewidths, and resonance intensities (ppm of the ion beam current). The +1.85 volts offset voltage is added to the measured resonance voltages to calculate the corrected resonance voltages, which then are used in Eq. (3) to calculate the transition intervals. The resonance intensities are expressed in ppm of the ion beam current. Due to the unknown saturation factor (the laser power is at partial saturation region), population distribution and detection efficiency (which may depend on the transition and beam voltage), those numbers are not an accurate account for resonance strength.

Table 4 Ion source pressure effect. The measured resonance voltages are fitted to a linear function of source chamber pressure.

a) Transition frequency = $1888.0654 \text{ cm}^{-1}$	
Source chamber pressure <sup>a</sup> ( $\times 10^{-5}$ Torr)	Measured resonance <sup>b</sup> voltage (volts)
1.15	+6775.10
2.00	+6775.15
4.00	+6775.30
5.60	+6775.60
7.80	+6775.55
9.80	+6775.80
Fitting slope = $0.08 \pm 0.03 \text{ volts}/10^{-5} \text{ Torr}$	
b) Transition frequency = $1811.6918 \text{ cm}^{-1}$	
Source chamber pressure <sup>a</sup> ( $\times 10^{-5}$ Torr)	Measured resonance <sup>b</sup> voltage (volts)
1.1	+4438.80
2.0	+4438.80
4.0	+4439.00
6.2	+4439.30
7.8	+4439.50
10.1	+4439.50
Fitting slope = $0.08 \pm 0.02 \text{ volts}/10^{-5} \text{ Torr}$	

<sup>a</sup> uncorrected ion gauge reading.

<sup>b</sup> uncertainty =  $\pm 0.15 \text{ volts}$ .

Full widths at half maximum (FWHM) of the resonances ranged from 15 to 22 MHz (corresponding to roughly a width of 2 to 3 volts in the beam voltage). A major contribution to the observed linewidths is the kinetic energy spread in the ion beam which arises from the ion-molecule reaction and also the space-charge potentials in the ion source and ion beam. Experiments<sup>54</sup> have shown that the kinetic energy spread of the  $\text{H}_3^+$  produced from  $\text{H}_2^+-\text{H}_2$  reaction could be larger than 1 eV. Smaller contributions include laser power broadening, laser linewidth, the angular divergences of the two intersecting beams and transient broadening effect. Hyperfine structure, estimated to be less than 1 MHz, is unresolved.

Although the transition frequency measurements are very reproducible, there are still errors in the calibration of them. Table 6 lists estimated contributions to the transition frequency measurement uncertainty.

The largest contribution to the calibration error is the laser

TABLE 5 Summary of the measurements of  $D_3^+$  vibrational-rotational transition frequencies. -- The value used for the  $D_3^+$  mass is 6.041756848(66) amu ( $Mc^2=5927.906$  MeV) as calculated from data given by Ref. 55.

No.	$^{12}C^{16}O$ -laser transition		$D_3^+$ Ion transition				
	$(v', N') - (v'', N'')$	Assumed frequency ( $cm^{-1}$ )	Corrected resonance voltage (V)	Observed frequency ( $cm^{-1}$ )	FWHM (MHz)	Resonance intensity (ppm)	Identification $(J, K)^d - (J, K)^e$ <sub>I, II</sub>
1	(16,20)-(15,21)	1676.8904	+3172.45	1678.6717	15	6.0	
2	(16,20)-(15,21)	1676.8904	+3202.25	1678.6801	16	7.2	
3	(17,13)-(16,14)	1679.2899	+6603.35	1681.8642	15	1.7	
4	(16,19)-(15,20)	1680.8786	+2989.60	1682.6119	15	1.6	
5	(15,15)-(14,16)	1721.3650	-6560.35	1718.7388	16	4.0	
6	(15,15)-(14,16)	1721.3650	-6496.45	1718.7517	17	0.6	
7	(16, 8)-(15, 9) <sup>a</sup>	1722.6043	-4383.35	1720.4558	16	5.4	
8	(13,19)-(12,20)	1755.2747	+4431.25 <sup>b</sup>	1757.4786	15	1.0 <sup>f</sup>	(2,0)-(1,0)
9	(14,12)-(13,13)	1757.8963	+1560.85 <sup>b</sup>	1759.2059	18	1.4 <sup>c</sup>	(2,1)-(1,1)
10	(13,18)-(12,19)	1759.3361	+5114.60 <sup>b</sup>	1761.7095	15	1.8 <sup>c</sup>	(2,2)-(1,2)
11	(12,14)-(11,15)	1800.3990	+3296.75	1802.3487	17	3.3	(1,1)-(0,1)
12	(11,19)-(10,20)	1805.2859	-6784.80	1802.4850	17	1.9	
13	(12,14)-(11,15)	1800.3990	+4657.85 <sup>b</sup>	1802.7167	15	1.0 <sup>c</sup>	(7,6)-(7,6) <sub>II</sub>
14	(11,19)-(10,20)	1805.2859	-3290.85	1803.3348	21	1.5	
15	(12,11)-(11,12)	1812.1026	-2940.10	1810.2514	18	2.7	
16	(12,12)-(11,13)	1808.2344	+4349.15 <sup>b</sup>	1810.4837	16	0.9 <sup>c</sup>	(6,5)-(6,5) <sub>II</sub>
17	(11,18)-(10,19)	1809.4175	+1928.85 <sup>b</sup>	1810.9161	15	1.5 <sup>c</sup>	(6,0)-(6,0)
18	(11,18)-(10,19)	1809.4175	+2498.65 <sup>b</sup>	1811.1232	15	1.1 <sup>c</sup>	(6,1)-(6,1) <sub>II</sub>
19	(11,18)-(10,19)	1809.4175	+4440.65 <sup>b</sup>	1811.6920	18	9.4	(6,2)-(6,2) <sub>II</sub>
20	(10,22)-( 9,23)	1817.7208	+2700.25	1819.5022	18	1.3 <sup>c</sup>	(5,1)-(5,1) <sub>II</sub>
	(11,16)-(10,17)	1817.5840	+3130.30	1819.5019	17	1.5 <sup>c</sup>	
21	(10,21)-( 9,22) <sup>a</sup>	1821.9831	-4045.10	1819.8000	19	0.6	
	(11,15)-(10,16) <sup>a</sup>	1821.6186	-2807.10	1819.8002	22	0.7	
22	(11,16)-(10,17)	1817.5840	+4325.45	1819.8387	15	1.3 <sup>c</sup>	(5,2)-(5,2) <sub>II</sub>
23	(11,16)-(10,17)	1817.5840	+4931.55	1819.9916	16	1.5 <sup>c</sup>	(5,3)-(5,3) <sub>II</sub>
24	(11,13)-(10,14)	1829.5899	-6974.75	1826.7119	15	2.1	
25	(11,13)-(10,14)	1829.5899	-5765.45	1826.9731	15	2.7	
26	(11,13)-(10,14)	1829.5899	-5756.75	1826.9750	16	3.1	



TABLE 5      Continued

27	(11,12)-(10,13)	1833.5262	-4253.10	1831.2736	20	8.5	(3,2)-(3,2) <sub>11</sub>
	(11,13)-(10,14)	1829.5899	+2381.35	1831.2737	20	6.5	
28	(10,18)-( 9,19)	1834.5792	-2709.15	1832.7801	19	4.0	
29	(10,18)-( 9,19)	1834.5792	+3501.75	1836.6268	22	17.3	
30	(10,18)-( 9,19)	1834.5792	+6714.55	1837.4151	17	0.6	
31	(10,16)-( 9,17)	1842.8158	-3409.55	1840.7885	18	0.7	
32	(10,15)-( 9,16) <sup>a</sup>	1846.8855	-5999.85	1844.1908	18	0.5	
	( 9,21)-( 8,22) <sup>a</sup>	1847.1185	-7081.65	1844.1908	16	0.4	
33	( 9,21)-( 8,22)	1847.1185	+2113.70	1848.7200	18	5.6	
34	( 9,20)-( 8,21)	1851.3842	-3139.20	1849.4299	17	7.0	
	(10,15)-( 9,16)	1846.8855	+5333.55	1849.4298	18	17.8	
	( 9,21)-( 8,22)	1847.1185	+4401.55	1849.4300	18	5.6	
35	(10,13)-( 9,14)	1854.9269	-4062.95	1852.6995	17	2.6	
	(10,14)-( 9,15)	1850.9226	+2590.85	1852.6994	18	10.0	
36	(10,12)-( 9,13)	1858.8982	-7677.05	1855.8305	15	4.1	
37	( 9,17)-( 9,18)	1863.9893	-6879.65	1861.0772	19	1.0	
	(10,12)-( 9,13)	1858.8982	+3862.55	1861.0772	22	0.6	
38	(10,12)-(19,13)	1858.8982	+5913.65	1861.5948	15	1.1	
39	( 9,17)-( 8,18)	1863.9893	-3218.80	1861.9969	19	5.6	
	(10,12)-( 9,13)	1858.8982	+7807.05	1861.9969	15	2.3	
	( 9,18)-( 8,19)	1859.8189	+3852.15	1861.9970	17	2.0	
40	( 9,18)-( 8,19)	1859.8198	+4411.35	1862.1497	15	1.1	
41	( 9,18)-( 8,19)	1859.8198	+6549.40	1862.6592	17	1.0	
42	( 9,18)-( 8,19)	1859.8198	+7500.60	1862.8585	16	1.7	
43	( 9,15)-( 8,16)	1872.2313	+6653.25	1875.1122	17	1.2	
44	( 8,18)-( 7,19)	1885.1378	+6776.80	1888.0654	16	1.0	
45	( 7,17)-( 6,18)	1914.7714	+6334.60	1917.6463	16	0.9	

<sup>a</sup> Laser was locked at single-mode.<sup>b</sup> Accuracy =  $\pm 0.5$  volts<sup>c</sup> Multiply the intensity by 4 in order to compare with other intensities. These scans were done before careful optimization.<sup>d</sup> Lower state.<sup>e</sup> Upper state.

frequency uncertainty. The principal cause is due to the shifts of the laser frequency with operating conditions. Assuming a value of 5 MHz/Torr pressure shift obtained by Laguna-Ayala<sup>57</sup>, an uncertainty of 10 MHz due to operating conditions is assigned. Lesser contributions arise from the uncertainty in laser stabilization and in the laser spectroscopic data<sup>56</sup>.

TABLE 6 Estimated contributions to experimental uncertainties. -- Assumed beam energy is 4000 eV and assumed transition frequency is  $1900 \text{ cm}^{-1}$  ( $5.7 \times 10^7 \text{ MHz}$ ).

Item	Assumed value	Contribution in MHz	Contribution in $\text{cm}^{-1}$	Fraction of transition frequency
Laser frequency uncertainty (stabilization accuracy)	3 MHz	3	$1.0 \times 10^{-4}$	$5.2 \times 10^{-8}$
Laser frequency uncertainty (spectroscopic data)	5 MHz	5	$1.7 \times 10^{-4}$	$8.8 \times 10^{-8}$
Laser frequency shifts with operating conditions	10 MHz	10	$3.3 \times 10^{-4}$	$18.0 \times 10^{-8}$
Potential offsets uncertainty	0.15 V	1.3	$0.4 \times 10^{-4}$	$2.1 \times 10^{-8}$
Beam voltage calibration	(100 ppm)	3.5	$1.2 \times 10^{-4}$	$6.1 \times 10^{-8}$
Line center estimate from chart	0.15 V	1.3	$0.4 \times 10^{-4}$	$2.1 \times 10^{-8}$
Quadratic sum		12.2	$4.0 \times 10^{-4}$	$2.2 \times 10^{-7}$

Another contribution includes the uncertainty in the line-center estimate, potential offsets, beam voltage measurements, and interaction angle. The resulting calibration error is about 12 MHz or  $0.0004 \text{ cm}^{-1}$  which is within 0.22 ppm of the transition frequency.

Four of the eight published  $\text{D}_3^+$  transitions<sup>14</sup> have been assigned by Carney and Ponter<sup>11</sup>. They made an adjustment of  $+8.9 \text{ cm}^{-1}$  in the vibrational frequencies and  $+1.6\%$  in the rotational energies of their ab initio results to obtain the best fit of the experimental values. The close agreement ( $0.03 \text{ cm}^{-1}$  maximum error) on all four assigned transitions confirms the assignments. Later, we observed three more transitions near (within  $0.65 \text{ cm}^{-1}$ ) one (No. 13 of Table 5) of those assigned transitions, the identification of this transition became uncertain. Recently, Watson<sup>58</sup> derived the molecular constants of  $\text{D}_3^+$  from  $\text{H}_3^+$  constants based on isotope relations, then, he tried to fit the observed spectrum by adjusting some constants. The preliminary results are included in Table 5, too.

The identification is still far from completeless, currently, Watson<sup>58</sup> is trying to fit the spectrum differently. In order to help this, we plan to observe the dependence of the transition intensities on the source pressure and see if there is any way to tell the transitions of the fundamental band from the others.

### B. $\text{HD}_2^+$

The experimental procedure and method of data analysis have been described in the previous section only the results will be discussed here.

The study of  $\text{D}_3^+$  transitions shows a constant potential offset (+1.85 volts) and source pressure shift (+0.08 volts/ $10^{-5}$  torr) on the measured resonance voltage. The results of potential offset for  $\text{HD}_2^+$  are listed in Table 7. The potential offset +2.30 volts is different from

TABLE 7 Summary of the study of potential offset for  $\text{HD}_2^+$ .

$^{12}\text{C}^{16}\text{O}$ -Laser transition		$\text{HD}_2^+$ Ion transition				
( $\nu', N'$ )-( $\nu'', N''$ )	Assumed frequency ( $\text{cm}^{-1}$ )	Measured resonance voltage (V)	Uncorrected frequency ( $\text{cm}^{-1}$ )	Offset voltage (V)	Corrected resonance voltage (V)	Resonance frequency ( $\text{cm}^{-1}$ )
( 9,18)-( 8,19)	1859.8198	-3867.92	1857.4330	2.24	-3870.22	1857.4323
(10,13)-( 9,14)	1854.9269	+4271.20	1857.4317		+4273.50	1857.4324
( 9,18)-( 8,19)	1859.8198	-3106.63	1857.6806	2.55	-3108.93	1857.6798
(10,13)-( 9,14)	1854.9269	+5155.85	1857.6971		+5158.15	1857.6797
( 8,18)-( 7,19)	1885.1378	-3292.99	1882.9055	2.50	-3295.30	1882.9047
( 9,13)-( 8,14)	1880.3427	+4345.70	1882.9039		+4348.00	1882.9046
( 8,15)-( 7,16)	1897.6545	-3220.55	1895.4322	1.98	-3222.85	1895.4314
( 8,16)-( 7,17)	1893.5147	+2399.20	1895.4307		+2401.50	1895.4316
average				2.32±0.26		
least-squares fit				2.30±0.16		



the  $D_3^+$  result. Since the offset depends on the source pressure, the difference may be due to this pressure effect. The source chamber pressure was measured by an ionization gauge and the reading (without correction by gauge factor) was kept roughly the same for all the experimental scans. It is possible the pressure is different for different gas mixtures even though the gauge reading is the same. The other possibility is that the kinetic energy distribution may be different for different ions<sup>54</sup> since they are produced by different channels of ion-molecule reaction (1).

The observed  $HD_2^+$  transitions are presented in Table 8. The potential offset of +2.30 volts is used for  $HD_2^+$ . The assigned uncertainty for  $HD_2^+$  is  $0.0004\text{ cm}^{-1}$  (2.2 ppm), and the observed linewidths for  $HD_2^+$  resonances ranges from 8 to 15 MHz. The contributions to the linewidths are similar to  $D_3^+$ .

No attempt to identify the observed  $HD_2^+$  has made yet. Due to the smaller vibrational frequencies of  $HD_2^+$  compared to  $H_2D^+$ , we believe we may already observe transitions with  $J$  as low as 1 or 0. We believe the identification of the observed  $HD_2^+$  transitions should be easier than  $H_2D^+$  (see later description).

### C. $H_2D^+$

There is no experimental results for potential offset since all the transitions have been observed with laser beam anti-parallel to the ion beam. The observed  $H_2D^+$  transitions are listed in Table 9. A potential offset of +2.1 volts, which is the averaged value of  $D_3^+$  and  $HD_2^+$  results, is used to calculate the correct resonance voltage. The assigned uncertainty in the center voltage is 0.5 volts, this increases the uncertainty of  $H_2D^+$  transition frequency to  $0.00045\text{ cm}^{-1}$  (2.4 ppm). The observed linewidth for  $H_2D^+$  resonance ranges between 12 and 16 MHz.

The preliminary results, based on ab initio calculations by Porter and Carney<sup>59</sup>, indicate that the rotational quantum number  $J$  of our observed transitions for  $H_2D^+$  has a range 2 to 8, i.e., we probably observed the transitions involved quite high  $J$ . However, there is a possible aid to identification, we note that some of the resonances listed in Table 9 occur in pairs, perhaps corresponding to the two different mutual orientations of the two protons. If this hypothesis is correct, the stronger line of each doublet would be a transition between ortho (spin triplet) states, and the weaker line would be a transition between para (spin singlet) states. The experimentally observed intensities are often reasonably close to the 3:1 ratio of saturated intensities from the ratio of statistical weights.

TABLE 8 Summary of the measurements of  $\text{HD}_2^+$  vibrational-rotational transition frequencies. -- The value used for  $\text{HD}_2^+$  mass is 5.035480089(45) amu ( $Mc^2=4690.5576$  MeV), as calculated from data in Ref. 55.

No.	$^{12}\text{C}^{16}\text{O}$ -laser transition		$\text{HD}_2^+$ Ion transition			
	(VU,JU)-(VL,JL)	Assumed frequency ( $\text{cm}^{-1}$ )	Corrected <sup>b</sup> resonance voltage (V)	Observed frequency ( $\text{cm}^{-1}$ )	FWHM (MHz)	Resonance intensity (ppm)
1	(12,18)-(11,19)	1784.3361	-3097.20	1782.2869	12	5.3
2	(12,17)-(11,18)	1788.4004	-3146.04	1786.3304	13	7.4
3	(11,19)-(10,20)	1805.2859	+3055.20	1807.3474	11	2.5
4	(12,11)-(11,12)	1812.1026	-4814.83	1809.5082	11	5.8
5	(11,18)-(10,19)	1809.4175	+3276.06	1811.5572	13	1.1
6	(10,18)-( 9,19)	1834.5792	-4495.57	1832.0411	11	11.5
7	(10,18)-( 9,19)	1834.5792	+5195.58	1837.3117	12	16.7
8	( 9,19)-( 8,20)	1955.6180	-4047.55	1853.1820	13	10.0
8	(10,14)-( 9,15) <sup>a</sup>	1854.9269	-2077.20	1853.1820	15	8.6
9	( 9,20)-( 8,21)	1851.3842	+5535.99	1854.2307	8	3.1
10	( 9,18)-( 8,19)	1859.8198	-3870.23	1857.4323	13	2.4
10	(10,13)-( 9,14)	1854.9269	+4273.54	1857.4324	13	1.9
11	(10,13)-( 9,14)	1854.9269	+5158.15	1857.6797	11	1.3
11	( 9,18)-( 8,19)	1859.8198	-3108.93	1857.6799	12	1.4
12	( 9,17)-( 8,18)	1863.9893	+5483.20	1866.8414	12	12.5
13	( 9,15)-( 8,16)	1872.2313	-3519.23	1869.9394	11	6.8
13	( 8,21)-( 7,22) <sup>a</sup>	1872.3313	-3832.15	1869.9396	12	7.1
14	( 9,13)-( 8,14)	1880.3427	-4565.01	1877.7213	12	2.3
15	( 9,13)-( 8,14)	1880.3427	-3050.51	1878.1995	12	4.0
15	( 8,19)-( 7,20)	1880.9009	-4844.76	1878.1996	13	5.4
16	( 8,18)-( 7,19)	1885.1378	-5871.11	1882.1577	12	1.9
17	( 8,18)-( 7,19)	1885.1378	-5700.54	1882.2012	14	7.0
18	( 9,13)-( 8,14)	1880.3427	+4348.00	1882.9046	12	1.6
18	( 8,18)-( 7,19)	1885.1378	-3295.29	1882.9047	13	2.5
19	( 8,18)-( 7,19)	1885.1378	+6505.15	1888.2798	11	7.6
20	( 8,18)-( 7,16)	1897.6545	-3624.70	1895.2970	13	3.9
21	( 8,15)-( 7,16)	1897.6545	-3222.85	1895.4314	14	3.6
21	( 8,16)-( 7,17)	1893.5147	+2401.55	1895.4317	12	2.2
22	( 7,17)-( 6,18)	1914.7714	-3640.59	1912.3874	13	17.1
23	( 7,16)-( 6,17)	1918.9788	-4076.19	1916.4507	13	5.0
24	( 7,17)-( 6,18)	1914.7714	+6082.20	1917.8572	12	11.3
25	( 6,18)-( 5,19)	1935.9999	-3028.75	1933.8012	14	0.9
26	( 6,17)-( 5,18)	1940.2747	+6048.15	1943.3929	11	1.8
27	( 6,15)-( 5,16) <sup>a</sup>	1948.7270	+6286.57	1951.9199	12	2.9
28	( 6,14)-( 5,15) <sup>a</sup>	1952.9043	+5240.20	1955.8255	12	3.3
29	( 5,18)-( 4,19) <sup>a</sup>	1961.5407	+3264.86	1963.8563	13	3.2
30	( 5,18)-( 4,19) <sup>a</sup>	1961.5407	+4459.17	1964.2472	14	1.3
31	( 5,18)-( 4,19) <sup>a</sup>	1961.5407	+5325.27	1964.4985	13	0.9

<sup>a</sup>Laser was locked at single mode.

<sup>b</sup>The potential offset of 2.30 volts is added to the measured resonance voltage. The sign before the resonance voltage represents the beam configuration: negative for parallel and positive for anti-parallel.

TABLE 9 Summary of the measurements of  $\text{H}_2\text{D}^+$  vibrational-rotational transition frequencies. -- The value used for  $\text{H}_2\text{D}^+$  mass is  $4.029203330(30)$  ( $Mc^2=3753.2092$  MeV) as calculated from data in Ref. 55.

No.	$^{12}\text{C}^{16}\text{O}$ -laser transition		$\text{H}_2\text{D}^+$ Ion transition			
	(VU,JU)-(VL,JL)	Assumed frequency ( $\text{cm}^{-1}$ )	Corrected <sup>a</sup> resonance voltage (V)	Observed frequency ( $\text{cm}^{-1}$ )	FWHM (MHz)	Resonance intensity (ppm)
1	(10,18)-( 9,19)	1834.5792	4992.10	1837.5737	12	1.9
2	(10,18)-( 9,19)	1834.5792	5379.00	1837.6876	12	0.8
3	( 8,17)-( 7,18)	1889.3424	5371.55	1892.5414	16	1.5
4	( 8,17)-( 7,18)	1889.3424	5426.48	1892.5577	14	3.8
5	( 8,16)-( 7,17)	1893.5147	3215.90	1895.9949	14	2.2
6	( 8,16)-( 7,17)	1893.5147	4186.40	1896.3448	13	1.1
7	( 6,19)-( 5,20)	1931.6929	3147.20	1934.1960	12	2.5
7	( 7,13)-( 6,14)	1931.4053	3912.65	1934.1960	13	2.4
8	( 7,13)-( 6,14)	1931.4053	5007.90	1934.5628	13	2.0
8	( 6,19)-( 5,20)	1931.6929	4136.75	1934.5629	13	2.7
9	( 6,15)-( 5,16)	1948.7270	5363.25	1952.0240	13	3.7

<sup>a</sup>The laser beam was antiparallel to the ion beam in all cases. An offset of 2.1 volts is added to the measured resonance voltage.

## V. Conclusion

This talk presents a detailed discussion of our experiment on the three deuterated species  $\text{H}_2\text{D}^+$ ,  $\text{HD}_2^+$  and  $\text{D}_3^+$ .

We expect that additional resonances will be found in the future since there are many ranges of the infrared spectral region presently accessible to our experimental apparatus have not been explored thus far. We also expect that the semi-empirical spectroscopic analysis by Watson<sup>58</sup> will soon assign most of the observed transitions of  $\text{D}_3^+$ . We hope that these results, combined with the results of Oka<sup>17,37</sup>, will lead to precise predictions of transitions observable in the interstellar medium in  $\text{H}_3^+$  and  $\text{H}_2\text{D}^+$  and also the assignment of the quantum numbers of the observed transitions of  $\text{H}_2\text{D}^+$  and  $\text{HD}_2^+$ .



## ACKNOWLEDGEMENTS

We are grateful to W.E. Lamb, Jr. for wise counsel, to R.N. Porter and G.D. Carney for sharing their theoretical calculations with us before publication. We wish to acknowledge useful conversations with A. Dalgarno, D. Dearborn, T. Oka, R. Saykally, P. Thaddeus, and W.D. Watson. Acknowledgment is also made to the donors of the Petroleum Research Fund, administered by the American Chemical Society, for partial support of this work. This work has also been partially supported by the National Science Foundation under Grant No. PHY79-15302. W.H.W. acknowledges support from the John Simon Guggenheim Memorial Foundation and the Alexander von Humboldt Foundation.

## REFERENCES

\* Present address: Department of Physics, National Tsing Hua University, Hsinchu, Taiwan 300, Republic of China.

† Present address: Department of Physics, University of Oregon, Eugene, Oregon 97403, U.S.A.

1. J.J. Thomson, *Phil. Mag.* 24, 209 (1912).
2. J.J. Thomson, *Proc. Roy. Soc. (London)* 89, 1 (1913).
3. A.J. Dempster, *Phil. Mag.* 31, 438 (1916).
4. T.R. Hogness and E.G. Lunn, *Phys. Rev.* 26, 44 (1925).
5. C.A. Coulson, *Proc. Cambridge Philos. Soc.* 31 (2), 244 (1935).
6. J. Hirschfelder, H. Eyring, and N. Rosen, *J. Chem. Phys.* 4, 121 (1936); 4, 130 (1936); J. Hirschfelder, H. Diamond, and H. Eyring, *J. Chem. Phys.* 5, 695 (1937); D. Stevenson and J. Hirschfelder, *J. Chem. Phys.* 5, 933 (1937); J.O. Hirschfelder, *J. Chem. Phys.* 6, 795 (1938).
7. G.S. Handler and J.R. Arnold, *J. Chem. Phys.* 27, 144 (1957).
8. L. Salman and R.D. Poshusta, *J. Chem. Phys.* 59, 3497 (1973); also the references therein.
9. G. Herzberg, *Sci. of Light* 16, 14 (1967); *Trans. Roy. Soc. Canada*, OV, 3 (1967).
10. G.D. Carney and R.N. Porter, *J. Chem. Phys.* 65, 3547 (1976); and *Chem. Phys. Lett.* 50, 327 (1977).
11. G.D. Carney and R.N. Porter, *Phys. Rev. Lett.* 45, 537 (1981); and private communication.
12. M.J. Gaillard, D.S. Gemmell, G. Goldring, I. Levine, W.J. Pietsch, J.C. Poizat, A.J. Ratkowski, J. Remillieux, V. Vager, and B.J. Zabransky, *Phys. Rev. A* 17, 1797 (1978).
13. G. Herzberg, *J. Chem. Phys.* 70, 4806 (1979).
14. J.-T. Shy, J.W. Farley, W.E. Lamb, Jr., and W.H. Wing, *Phys. Rev. Lett.* 45, 535 (1980).
15. W.H. Wing, G.A. Ruff, W.E. Lamb, and J.J. Spezeski, *Phys. Rev. Lett.* 36, 1488 (1976).
16. D.E. Tolliver, G.A. Kyrala, and W.H. Wing, *Phys. Rev. Lett.* 43, 1719 (1979).
17. T. Oka, *Phys. Rev. Lett.* 45, 531 (1980).
18. J.-T. Shy, J.W. Farley, and W.H. Wing, *Phys. Rev. A* 24, 1146 (1981).
19. J.-T. Shy, J.W. Farley, R. DeSerio, and W.H. Wing, Abstract, 182nd National Meeting of the American Chemical Society, New York, New York, Aug. 23-28, 1981.
20. E. Herbst and W. Klemperer, *Astrophys. J.* 185, 5050 (1973); *Phys. Today*, June 1976, p.32.
21. W.D. Watson, *Rev. Mod. Phys.* 48, 513 (1976).
22. T. deJong, A. Dalgarno, and W. Boland, *Astron. Astrophys.* 91, 68 (1980).
23. H. Suzuki, *Prog. Theor. Phys.* 62, 936 (1979)..

24. W.D. Watson, in CNO Isotopes in Astrophysics, edited by Jean Andouze (Reidel, Dordrecht, 1976), p. 105.
25. M. Guelin, W.D. Langer, R.L. Shell, and H.A. Wooten, *Astrophys. J.* 217, L165 (1977).
26. P. Angerhofer, E. Churchwell, and R.N. Porter, *Astrophys. Lett.* 19, 137 (1978).
27. T. Oka: "Molecules in Interstellar Space", The Royal Society Meeting for Discussion, London, May (1981).
28. G.F. Mitchell, J.L. Ginsburg, and P.L. Kunta, *Astrophys. J.* 212, 71 (1977).
29. S.S. Prasad and A. Tan, *Geophys. Res. Lett.* 1, 337 (1979).
30. D. Lupu and V. Bucur, *J. Phys. Chem. Solids*, 38, 387 (1977).
31. G.D. Carney, *Mol. Phys.* 39, 923 (1980).
32. D.L. Smith and J.H. Futrell, *Chem. Phys. Lett.* 24, 611 (1974); *J. Phys. B* 8, 803 (1975); A.S. Fiaux, D.L. Smith, and J.H. Futrell, *Int. J. Ion Phys. Mass Spectrom.* 20, 223 (1976); *J. Am. Chem. Soc.* 98, 5773 (1976).
33. I. Dabrowski and G. Herzberg, *Can. J. Phys.* 58, 1238 (1980); G. Herzberg, H. Lew, J.J. Sloan, and J.K.G. Watson, *Can. J. Phys.* 59, 428 (1981); G. Herzberg and J.K.G. Watson, *Can. J. Phys.* 58, 1250 (1980) therein.
34. H. Figger, H. Moller, W. Schrepp, and H. Walther, *Chem. Phys. Lett.* 90, 90 (1982).
35. R.C. Woods, *Rev. Sci. Instrum.* 44, 282 (1973).
36. A.S. Pine, *J. Opt. Soc. Amer.* 64, 1683 (1974), 66, 97 (1976).
37. T. Oka, in Laser Spectroscopy V, edited by A.R.W. McKellar, T. Oka, and B.P. Stoicheff (Springer-Verlag, New York, 1981), pp. 320-323.
38. A. Carrington, J. Buttenshaw, and R. Kennedy, *Mol. Phys.* 45, 753 (1982).
39. W.H. Wing in Laser Spectroscopy III, edited by J.L. Hall and J.L. Carlsten (Springer, New York, 1977), pp. 69-75.
40. J.J. Spezeski, G.A. Ruff, and W.H. Wing, *Rev. Sci. Instrum.*, 49, 1327 (1978).
41. G.A. Kyrala, D.E. Tolliver, and W.H. Wing, *J. Ion Phys. Mass. Spectrom.* 33, 367 (1980).
42. J.J. Leventhal and Friedman, *J. Chem. Phys.* 49, 1974 (1968); 50, 2928 (1969).
43. W.T. Huntress, Jr. and M.T. Bowers, *Int. J. Ion Phys. Mass Spectrom.* 12, 1 (1973); M.T. Bowers, W.J. Chesnavich, and W.T. Huntress, Jr., *Int. J. Ion Phys. Mass. Spectrom.* 12, 357 (1973); J.K. Kim, L.P. Theard, and W.T. Huntress, Jr., *Int. J. Ion Phys. Mass. Spectrom.* 15, 223 (1974).
44. N.G. Adams and D. Smith, *Ap. J.* 248, 373 (1981).
45. G.W. McClure, *Phys. Rev.* 130, 1852 (1963).
46. J.F. Williams and D.N.F. Dunbar, *Phys. Rev.* 149, 62 (1966).
47. E.S. Chambers, *Phys. Rev.* 139, A1068 (1965).
48. B. Peart and K.T. Dolder, *J. Phys. B* 7, 1567 (1974).
49. S.L. Kaufman, *Opt. Commun.* 17, 309 (1976).



50. C. Freed, IEEE J. Quantum Electron. QE-4, 404 (1968); Appl. Phys. Lett. 18, 485 (1971); and private communications.
51. R. DeSerio, G.A. Ruff, and W.H. Wing (to be published).
52. D. Djeu, Appl. Phys. Lett. 23, 309 (1973).
53. A. Yariv, Quantum Electronics (John Wiley and Sons, Inc., New York, 2nd edition, 1975) Eq. (7.3-6).
54. C.H. Douglass, D.J. McClure, and W.R. Gentry, J. Chem. Phys. 67, 4931 (1977); and the references therein.
55. E. Richard Cohen and B.N. Taylor, J. Phys. Chem. Ref. Data 2, 663 (1973).
56. R.M. Dale, M. Herman, J.W.C. Johns, A.R.W. McKellar, S. Naglev, and I.K.M. Strathy, Can. J. Phys. 57, 677 (1979).
57. A.G. Laguna-Ayala, M.S. thesis, University of Arizona, 1979 (unpublished).
58. J.K.G. Watson, private communications.
59. G.D. Carney and R.N. Porter, private communication.